Demirel *et al. Energy Informatics* (2025) 8:32
https://doi.org/10.1186/s42162-025-00489-6

Energy Informatics

RESEARCH Open Access

PIDE: Photovoltaic integration dynamics and efficiency for autonomous control on power distribution grids

Gökhan Demirel[1*], Natascha Fernengel[1], Simon Grafenhorst[1], Kevin Förderer[1] and Veit Hagenmeyer[1]

*Correspondence:
Gökhan Demirel
goekhan.demirel@kit.edu
[1]Institute for Automation and Applied Informatics, Karlsruhe Institute of Technology, Hermann-von-Helmholtz-Platz 1, Eggenstein-Leopoldshafen 76344, Germany

Abstract

With a focus on larger rooftop or utility-scale solar systems, there is a lack of research on the potential impact of mini photovoltaic (MPV) systems, often referred to as balcony power plants. This work analyzes the impact of varying concentrations of MPV systems, on the stability and control of low-voltage (LV) grids. We offer a comprehensive technical assessment of MPV within a distribution grid and quantify their effects on power quality, losses, transformer loading, and the performance of other inverter-based voltage-regulation devices. For this purpose, this paper introduces the open-source Python-based framework PIDE (Photovoltaic Integration Dynamics and Efficiency), a tool for simulating the integration of distributed energy resources (DER)s and evaluating their impact on autonomous reactive power control in the distribution grid. Our case studies include a one-year sensitivity analysis based on Monte Carlo simulations, compare distributed and decentralized DER control strategies, and demonstrate the role of autonomous inverters in providing ancillary services. With the growing use of battery energy storage (BES) systems in LV grids for these services, the need for adaptable DER control strategies becomes increasingly evident. Our results show that high MPV penetration increases mean transformer load by up to 3%, line load by 2.5% and total power losses by around 17%.

Keywords Battery energy storage, Distributed energy resources, Mini photovoltaic systems, Voltage control, Sensitivity analysis, Monte carlo experiments, Configuration optimization

Introduction

Balcony power plants, referred to in this paper as mini photovoltaic (MPV) systems, are a pioneering innovation by Holger Laudeley in Germany and worldwide in the early 2000s [56]. Since then, their prevalence has grown exponentially. His vision of portable and easily installed mini balcony power units has become a significant trend in the renewable energy sector. In 2025, an estimated 700,000 MPV systems will be used in Germany, with a total capacity of around 500 MW [13]. Schmitz et al. [48] present a practical guide for their application. Furthermore, photovoltaic (PV) systems constitute approximately 45% of the total installed renewable energy capacity of 150 GWp [11]. To further promote the adoption of these systems, German Association for Electrical, Electronic & Information Technologies (VDE) has proposed amendments, including raising the maximum power to 800 Wp and implementing a regulation allowing meters to run backward within this limit. These proposed changes align with European Network Code on Requirements for Generators (NC RfG)), as described in [22] and [46], and are expected to increase the penetration rate of plug-and-play MPV systems. Several European countries, including Belgium, Cyprus, Denmark, Italy, and the Netherlands, have adopted net metering as standard practice [26, 42]. Moreover, 44 states in the US also use this approach [21]. This widespread use highlights the global importance of the German households VDE changes.

With solar panels achieving grid parity for many households Bergner et al. [8], the self-consumption of locally generated PV electricity has become more economically viable than relying on feed-in tariffs into the electrical grid [12]. Using battery energy storage (BES) systems further amplifies this advantage [27]. As a result, the economic appeal and straightforward integration of local balcony power plants encourage more investment in households. The prospects for widespread adoption of MPV systems are positive. Active research and progressive regulatory changes are addressing issues such as grid stability, safety concerns, and end-of-life panel management, continually improving the viability and sustainability of these systems [8, 11, 22, 46].

This paper explores the complex dynamics of LV grid operation with an increasing penetration and integration of MPVs and distributed energy resources (DERs), considering their interactions with other DERs. As the global community steers toward a sustainable future, comprehending the consequences of assimilating innovative energy sources gains significance. Expectations are that gaining insights into these dynamics will illuminate critical aspects of operational stability, safety, and efficiency in power systems, especially at the LV grid level. These insights are currently scarce as MPVs are a relatively new kind of DER that only recently started to gain traction and with seemingly little impact. By addressing the following main research questions, we aim to illuminate and outline the outcomes of such an integration.

The questions serve as guiding posts for the study. They are intended to shed light on potential impacts while offering fundamental strategies for optimizing and controlling power systems amidst growing MPV and DER integration:

1. **RQ1:** What are the effects of increasing MPV and DER integration on grid stability and reverse power flow, considering the radial topology of LV grids?
2. **RQ2:** How does MPV integration at the Point of Common Coupling (PCC) influence voltage rise in LV grids?
3. **RQ3:** Which inverter control strategies (e.g., $Q(V)$, $Q(P)$), and grid control approaches (e.g., decentralized and distributed) are most effective in optimizing self-consumption and maintaining grid stability in the face of increasing MPV penetration?

This work compares decentralized and distributed grid control strategies for active voltage control and outlines future research directions. Our environment is using PandaPower [55] and SimBench [36]. With our configurable framework, we integrate small MPVs and support configurable grid topologies and DER sizes. This research aims to contribute to the renewable energy sector and electrical grid management concerning MPV integration. The findings provide guidances for strategies for leveraging these uncertain MPVs and DERs due to weather-dependent power generation while ensuring grid stability and safety. This paper is a significantly extended version of our previous publication presented at the 4th Energy Informatics Academy Conference (EI.A 2024) [18]. The main contributions of this paper are as follows:

- We present PIDE[1], an open-source Python-based framework that implements the VDE-AR-N 4105 guidelines. The framework facilitates the decentralized provision of ancillary services (active and reactive power) at DER inverter terminals.
- We discuss challenges associated with MPVs, evaluate rule-based and time-of-day BES control strategies, and different BES sizing to mitigate congestion and enhance operator profit across various DER penetration configurations in LV grids.
- We conduct real-world time series data analysis and simulations across various LV grid topologies ranging from small rural (15-bus) to large urban configurations (59-bus). We also provide the extended MPVBench dataset of real-time MPV data for the energy community with associated metadata, which contains detailed information on the hardware components.

The structure of this paper is as follows: Section "Related work addresses" challenges and solutions in active voltage regulation. Section "Background" outlines the regulatory framework for the European electrical grid system. In Section "Active voltage control problem statement", we define the active voltage control problem. Section "Electrical system environment" delves into BES uncertainty modeling and introduces Monte Carlo simulations to analyze the influence of MPVs on voltage regulation in LV grids. Section "Control strategies for distributed energy resources systems" explores Grid Code's local DER control modes, followed by diverse DER control strategies. Section "Experimental settings" presents the experimental settings, data and grid topology description, and performance metrics description of our grid control evaluation environment. Section "Results and discussion" presents the Monte Carlo results based on the setups from Sections "Experimental settings" and "Monte Carlo methods for electrical grid system simulations". Finally, Section "Conclusion" outlines the main conclusions and future research directions.

Related work

As the twilight of traditional grids approaches, the voltage control problem has been gaining momentum due to the increased integration of distributed resources like rooftop PVs [40]. Despite a declining growth rate, Germany is among the leading countries in installed PV capacity per capita, catalyzing further research endeavors for future high PV penetration configurations [53]. Voltage rise in distribution systems with small generators has been a focus for over two decades [34]. Decentralized power generation in LV grids can cause reversed load flow and overvoltages, which can be mitigated by the reactive power consumption of voltage source converters (VSCs) [31]. Cloud-induced transients in PV power can cause voltage flicker or excessive operation of voltage regulating equipment [4]. However, high PV penetration does not adversely impact grid voltage when distributed PV resources do not exceed an average of 2.5 kW per household on a typical distribution grid [57]. While they focus only on PVs, we analyze MPVs in the LV grid to highlight their impact on grid dynamics and challenges in grids with various

[1] PIDE is accessible at https://github.com/KIT-IAI/PIDE.

penetrations of DERs. Active and reactive power control strategies can effectively mitigate voltage rise and expand LV grid capacity [51]. Local PV storage and voltage control strategies also enhance PV grid integration [3], while autonomous voltage control strategies can defer grid reinforcement for economic benefits [52]. Both [30] and [63] propose coordinated control strategies using PV and BES systems to regulate voltage in LV grids with high PV penetrations. [30] shows that reactive PV inverters in combination with BES systems can control voltage rise and drop issues with a droop-based method. Conversely, [63] targets voltage rise during peak PV generation and voltage drop during peak load. The voltage profile of a distribution feeder under high PV penetration, as per Brazilian regulations, is analyzed in [59]. A voltage sensitivity analysis similar to Demirok et al. [19] is necessary to determine optimal configuration parameters like critical voltage values. Furthermore, [35] observed an increase in voltage rise with higher DER penetration levels, attributing this to the line impedance. Notably, the most distant DER integration may cause the highest voltage rise [49]. Moreover, the X/R ratio of a LV distribution grid line is relatively low, so neither the active (RP) nor the reactive terms (XQ) are negligible, and these terms can influence the voltage level at PCC [34]. In [9] introduces a single-phase inverter with reactive power control, as also highlighted in [61], which presents a hybrid modulation method for single-phase DC-AC conversion within new grid codes for ancillary services. In [45], a combination of a local and a distributed cooperative reactive power controller with a dynamic leader approach that tracks the position of the critical bus is shown for the coordination of all PVs for voltage regulation. Recent work has introduced a revised consensus algorithm for real-time reactive power control of distributed inverters [62] and a fully distributed bi-level optimization method for LV grids [29]. In addition, a distributed control strategy is being developed based on the local measurement and communication of neighboring buses [43].

While previous works on PV grid integration focus on large-scale solar systems, including reactive power strategies (e.g., [31, 51]), distributed control (e.g., [45, 63]), and autonomous voltage regulation (e.g., [3, 52, 52]), they neglect the dynamics of small balcony power plant systems. In contrast, our PIDE framework performs sensitivity analyses of MPV penetration levels and quantifies local grid impacts such as voltage instability and power losses. It also uses grid code conforming, autonomous inverter reactive power modes that follow technical standards. In contrast to the unpublished sources used in the named previous works, PIDE provides reproducibility and applicability. It allows researchers and grid operators to test decentralized/distributed grid control strategies under one-year Monte Carlo scenarios while providing a transparent platform for future grid code evolution.

Background

System architecture

Figure 1 visually represents relationships and the transformation of the European Power System. This transformation enables the grid to supply electricity and ancillary services to its users and the primary grid, as depicted by the bidirectional power flows. Administrative units, typically the Distribution System Operator (DSO), monitor and operate these PV systems via communication channels. Driven by recent changes in European grid code, the fast and seamless integration of balcony power plants into existing systems has become possible through plug-and-play technology using household sockets.

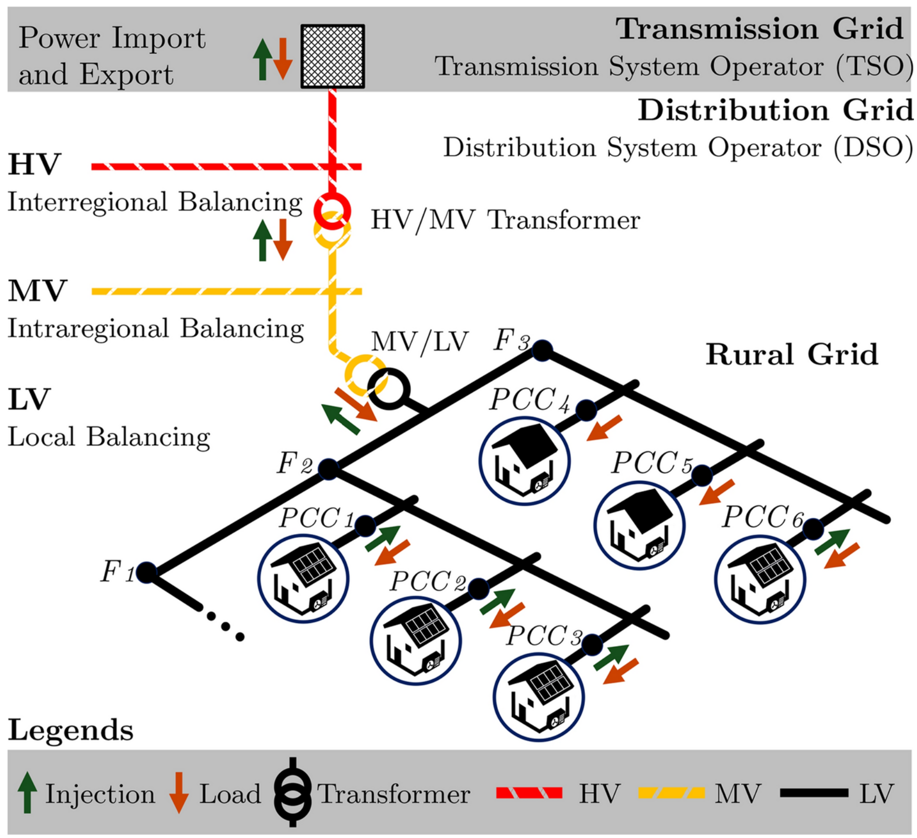

Fig. 1 Illustration of the European Power System showing interactions and connections via transformers between the transmission grid, inclusive of extra high voltage, the distribution grid, comprising high-voltage (indicated in red), medium-voltage (shown in yellow), and LV (represented in black). Power absorption is depicted in red arrows, while power injection into the higher and lower levels is indicated with green arrows

In Section "Experimental settings", we will consider different MPV parameterizations in the LV grid. We then perform a sensitivity analysis to evaluate the influence of MPV parameters on the electrical grid.

Regulatory framework

In Germany, the regulations and technical guidelines for static voltage stabilization comply with the voltage quality limits specified in the standards EN 50160 and the VDE application guideline VDE-AR-N 4105. This regulatory standard applies to the grid operation of DERs in the LV grid. The LV grid operates at a voltage level of $V_{\mathrm{LV}} \leq 1$ kV and has a nominal grid voltage ($V_{\mathrm{nom}} = 230$ V). The DSO allows DERs to operate within EN 50160's defined limits of 0.85 to 1.10 volts per-unit (p.u.) from the nominal voltage during undisturbed grid operation; otherwise, they automatically disconnect from the grid. EN 50160 defines that the root mean square (RMS) of the 10-minute average voltage shall ensure that the voltage range remains within $V_{\mathrm{nom}} \pm 10\%$ for 95% of each week [17]. DSOs adhere to this standard and ensure that voltage drops between lines and transformers remain within this range. VDE-AR-N 4105 mainly defines a regulation that allows a maximum voltage rise of 3% at each PCC due to DER installations in LV grids. DSOs prescribe methods for the feed-in of reactive power for static voltage stabilization at the terminals of the inverter-based DER [60]. In addition, the PIDE framework can also be adapted to a wide range of international regulations. For instance, IEEE

1547–2018 (North America) and the UK Engineering Recommendation G99, which contain very similar requirements for voltage and reactive power control [23, 28].

Active voltage control problem statement

We consider the LV distribution grid (represented in black) in Fig. 1 with arbitrary topologies as a graph $\mathcal{G} = (\mathcal{V}, \mathcal{E})$ with a set of nodes (buses) $\mathcal{V} = \{0, 1, \ldots, n\}$ with $n \in \mathbb{N}^{+}$. Each element of the set of edges (or lines) $\mathcal{E} = \{1, \ldots, n\}$ is a pair of nodes $\mathcal{E} \subseteq \mathcal{V} \times \mathcal{V}$. A typical European LV grid is characterized by a three-phase radial topology. In the present paper, we simplifiy the European LV grid to a single-phase system, representing it as a tree graph of $n+1$ buses. The bus indexed with 0 denotes the tree's root, representing the primary slack or substation bus connected to the superior electrical grid level. It regulates and balances the active and reactive power within the LV grid. This bus V_0 typically maintains a fixed reference voltage. Let $\mathcal{E}_{\pi(j)} \subseteq \mathcal{V}$ be the set of all nodes that are parents to the node *j* and $\mathcal{E}_{\sigma(j)} \subseteq \mathcal{V}$ the set of all nodes that are children of the node *j*. The complex power flowing from bus *i* to bus *j* is denoted by $S_{ij} = P_{ij} + \mathrm{j}Q_{ij}$, and can be decomposed into its active (P_{ij}) and reactive (Q_{ij}) components. At each bus $i \in \mathcal{V}$, V_i and θ_i denote the magnitude and phase angle of the complex voltage. Let $s_j = p_j + \mathrm{j}q_j$ be the net complex power injection at bus *j*. In this context, Tellegen's theorem, an offshoot of Kirchhoff's laws, elucidates the interrelationships between generated power, load flow, net power injection, and power transmission to and from bus *j* and its adjacent buses:

$$p_j = p_j^{\mathrm{G}} - p_j^{\mathrm{C}} = p_j^{\mathrm{MPV}} + p_j^{\mathrm{PV}} + p_j^{\mathrm{BES}} - p_j^{\mathrm{Load}} = p_j^{\mathrm{T}} \quad \forall j \in \mathcal{V}, \tag{1}$$

$$q_j = q_j^{\mathrm{G}} - q_j^{\mathrm{C}} = q_j^{\mathrm{MPV}} + q_j^{\mathrm{PV}} + q_j^{\mathrm{BES}} - q_j^{\mathrm{Load}} = q_j^{\mathrm{T}} \quad \forall j \in \mathcal{V}, \tag{2}$$

where terms p_j and q_j denote local generation by MPV and PV as well as BES discharging at node *j* minus local loads and BES charging, which is included in p_j^{BES} and q_j^{BES}. High levels of active power generation p_j can lead to voltage spikes, while a deficit may lead to voltage drops. DER-based inverters regulate the exchange of reactive power q_j on each bus to counteract these voltage fluctuations through reactive power management. Effective reactive power control ensures grid voltage stability by compensating for undesired voltage fluctuations. PV and BES systems are inverter-based DER units, while MPV systems only supply active power. The active and reactive power of BES systems, symbolized as p_j^{BES} and q_j^{BES}, can be exported to or imported from the grid. Energy exchange in the BES follows the relationship $p_j^{\mathrm{BES}} = p_j^{\mathrm{BES,dis}} + p_j^{\mathrm{BES,cha}}$, in which the term $p_j^{\mathrm{BES,dis}} \geq 0$ denotes the discharging power (energy injection into the electrical grid) and $p_j^{\mathrm{BES,cha}} \leq 0$ the charging power (energy absorption from the electrical grid). This sign convention is used for DERs and clarifies that we consider energy provision as positive and energy consumption as negative. For loads, a positive value signifies energy consumption from the electrical grid. The total DER reactive power, denoted by ($q_j^{\mathrm{DER}} = +q_j^{\mathrm{PV}} + q_j^{\mathrm{BES}}$), has a dual influence on voltage. Similarly, the active power is represented by p_j^{DER}. When the reactive power is in the underexcited state, which is characterized by the absorption of reactive power ($-q_j^{\mathrm{DER}}$), there is a drop in voltage due to inductive consumption. On the other hand, the injection of reactive power ($+q_j^{\mathrm{DER}}$) in the overexcited state leads to a rise in voltage due to the capacitive consumption of the DER inverters. Contrarily, loads absorb active and reactive power, captured by p_j^{Load} and q_j^{Load}. In cases where the bus *j* has no load, we assume them to be zero. Similarly, we directly zero the respective values in the absence of MPV, PV, or BES generation at bus *j*. Power flow problems describe the full non-linear AC power flow Eqs. and are essential for grid calculation and control.

Two fundamental formulations play a role here and are equivalent to each other: The power flow Eqs., formally known as the Bus Injection Model (BIM), is equivalent to the Branch Flow Model (BFM) [54]. Building on these fundamentals, the relaxed BFM Eqs. are as follows [25]:

$$p_j = \sum_{i \in \mathcal{E}_{\pi(j)}} (r_{ij} l_{ij} - P_{ij}) + \sum_{k \in \mathcal{E}_{\sigma(j)}} P_{jk}, \quad \forall j \in \mathcal{V}, \tag{3}$$

$$q_j = \sum_{i \in \mathcal{E}_{\pi(j)}} (x_{ij} l_{ij} - Q_{ij}) + \sum_{k \in \mathcal{E}_{\sigma(j)}} Q_{jk}, \quad \forall j \in \mathcal{V}, \tag{4}$$

$$V_j^2 = V_i^2 - 2(r_{ij}P_{ij} + x_{ij}Q_{ij}) + (r_{ij}^2 + x_{ij}^2) l_{ij}, \quad \forall (i,j) \in \mathcal{E}, \tag{5}$$

$$l_{ij} = \frac{P_{ij}^2 + Q_{ij}^2}{V_i}, \quad \forall (i,j) \in \mathcal{E}, \tag{6}$$

where V_j is the voltage at the PCC node *j*, and $z_{ij} = r_{ij} + \mathrm{j}x_{ij}$ represents the impedance z_{ij} described by the resistance r_{ij} and reactance x_{ij} on the line connecting buses *i* and *j*. Fig. 2 visually represents Eqs. (3-6) and illustrates the power flow relationships within the equivalent circuit of a LV grid. In this context, $\mathcal{F} = \{F_1, F_2, F_3\}$ denotes the set of feeders. Based on Kirchhoff's current and voltage laws, the first two Eqs. (3) and (4) balance active and reactive power. Ohm's law is the base for Eq. (5), and Eq. (6) that defines l_{ij} as the squared magnitude of the complex branch current on the line from bus *i* to *j*.

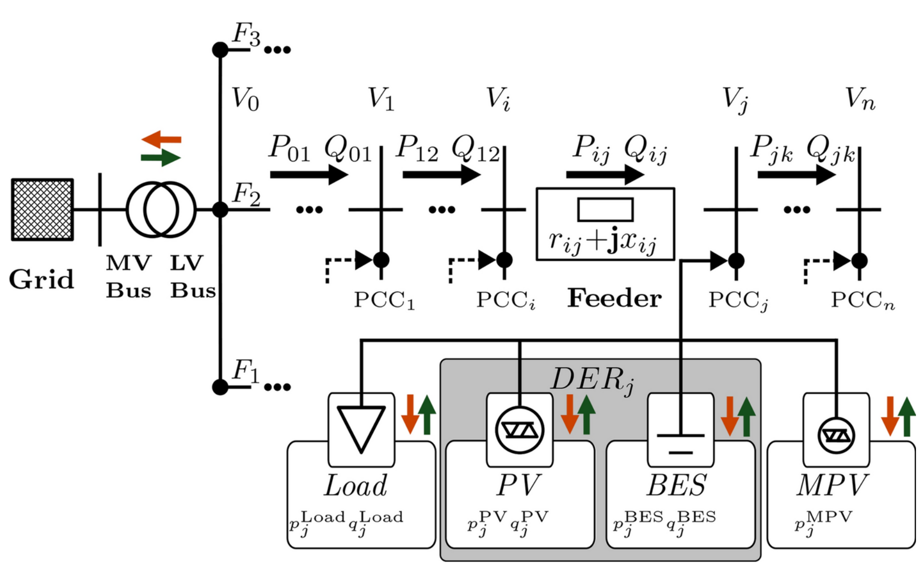

Fig. 2 Equivalent circuit of a radial electrical distribution system including loads, PVs, BESs, and MPVs. DER installations (PV and BES) with grey-shaded frames provide reactive power ancillary services. The distribution grid ranges from reference Bus 0 to Bus n

Control constraints

From the regulatory perspective, among the five local components contributing to $p_j + \mathrm{j}q_j$, four—namely p_j^{Load}, p_j^{MPV}, p_j^{DER}, and q_j^{Load} — are given uncontrollable quantities. Instead inverter-based DER control algorithms actively regulate the dynamics of reactive power flow q_j^{DER}, crucial for maintaining the voltage stability of the power grid. The transmission of reactive power is limited by technical constraints, making local DERs an effective solution for voltage regulation in LV grids. The reactive power control indirectly influences the active power p_j^{DER}, with the separate inverter apparent powers for PV (s_j^{PV}) and BES (s_j^{BES}) systems determining the operating constraints:

$$\left|q_j^{\mathrm{DER}}\right| \leq \sqrt{(s_j^{\mathrm{PV}})^2 - (p_j^{\mathrm{PV}})^2} + \sqrt{(s_j^{\mathrm{BES}})^2 - (p_j^{\mathrm{BES}})^2} \tag{7}$$

Equation (7) represents two inverters, one for the PV system and one for the BES system. For instance, assume a PV inverter rated at 13 kVA and a BES inverter at 10 kVA. If the PV inverter generates 5 kW, it still has a reactive capacity of $\sqrt{13^2 - 5^2} = 12\,\mathrm{kVAr}$. If the BES inverter supplies 8 kW, this gives $\sqrt{10^2 - 8^2} = 6\,\mathrm{kVAr}$. Together they can provide about 18 kVAr for voltage regulation. Nevertheless, when the active power of an inverter increases, its reactive power capacity decreases. This shows how the active and reactive power limits in Eq. (7) constrain real-world system operation.

The voltage drop $\Delta V_{ij} = V_i - V_j$ across a distribution line connecting nodes *i* and *j* can be approximated using the relationship [31]:

$$\Delta V_{ij} = \frac{r_{ij}\left(p_j^{\mathrm{Load}} - p_j^{\mathrm{DER}}\right) + x_{ij}\left(q_j^{\mathrm{Load}} - q_j^{\mathrm{DER}}\right)}{V_j} \tag{8}$$

where V_i is the parent busbar's voltage, which serves as a reference value. The terms r_{ij} and x_{ij} denote the resistance and reactance, respectively, between buses i and j as shown in Fig. 2. Such voltage deviations mainly depend on the impedance of the distribution line in combination with the dynamics of the active power feed-in [2]. Given Eq. (8), we describe the active power loss of the distribution line *j* connecting buses *i* and *j* as follows [7, 58]:

$$P_j^{\mathrm{loss}} = \frac{\left(p_j^{\mathrm{Load}} - p_j^{\mathrm{DER}}\right)^2 + \left(q_j^{\mathrm{Load}} - q_j^{\mathrm{DER}}\right)^2}{V_i^2} \cdot r_{ij} \tag{9}$$

Two pivotal objectives that dominate the global characteristics of electrical distribution grids are maintaining voltage regulation and minimizing active power losses. The primary goal is to maintain the voltage regulation within a certain range to ensure safe and optimal operation. We can express these voltage range constraints:

$$V_0 - \epsilon_v \leq V_j \leq V_0 + \epsilon_v \quad \forall j \in \mathcal{V} \quad \mathrm{p.u} \tag{10}$$

where ϵ_v is approximately 0.05 p.u., as described in Section "Regulatory framework". During nocturnal high-load intervals, the end consumer voltage can drop below 0.95 p.u., which represents an increased demand for electricity [1]. Conversely, in situations with significant feed-in from p_j^{DER}, the electricity export process leads to a reverse current flow that causes V_j to voltage rise over its nominal range [34]. This dichotomy underscores the inherent challenges of balancing power generation with consumption patterns. The total active power losses in the LV grid, which correspond to the aggregated line losses from Eq. (9), are given by [6, 7]:

$$\mathcal{P}^{\text{loss}} = \sum_{i=0}^{n-1} r_{ij} \frac{(P_{ij}^2 + Q_{ij}^2)}{V_i^2} = \sum_{i=0}^{n-1} r_{ii} l_{ij}^2 \quad \text{p.u.} \tag{11}$$

where $\mathcal{P}^{\text{loss}}$ denotes the total active power loss in the grid. Minimizing this loss is a secondary yet paramount objective in the electrical distribution grid.

Electrical system environment

This section focuses on electrical grid dynamic behavior and uncertainties, focusing on the BES models, Monte Carlo (MC) methods, and configurable MPV parameter settings. Section "Battery energy storage system model with uncertainty" introduces the BES model, addressing energy balance equations, stochastic uncertainties, and operational constraints for grid-connected storage systems. Section "Monte Carlo methods for electrical grid system simulations" describes applying MC methods to analyze uncertainties and evaluate the robustness of grid control strategies. Finally, Section "Influence of the configurable mini photovoltaic rates" analyzes the influence of configurable MPV rates on the performance and stability of LV grids. For simplicity, we focus on the temporal dynamics of the system and omit the distribution node index *j*. All equations are denoted with a subscript *t* to indicate time-dependent variables.

Battery energy storage system model with uncertainty

A typical BES system is designed with two main goals: to be economically efficient and to operate within grid constraints. This design aims to optimize self-consumption for the system owners. The charging and discharging power of the BES are derived from the net power p_t^{BES} as follows:

$$|p_t^{\text{cha}}| = \max(0, -p_t^{\text{BES}}), \quad |p_t^{\text{dis}}| = \max(0, p_t^{\text{BES}}), \tag{12}$$

combined with Eq. (13) ensure that charging and discharging are mutually exclusive:

$$|p_t^{\text{cha}}| \cdot |p_t^{\text{dis}}| = 0, \quad \text{where} \quad |p_t^{\text{cha}}| \geq 0 \quad \text{and} \quad |p_t^{\text{dis}}| \geq 0. \tag{13}$$

This implies that at any given time step t, if p_t^{BES} has negative values (indicating that the battery is charging, i.e., $|p_t^{\text{cha}}| \geq 0$) for energy consumption, then $p_t^{\text{dis}} = 0$, and vice versa. In a real system, a battery cannot charge and discharge simultaneously; hence, the mutual exclusion constraint in Eq. (13) ensures that only one of p_t^{cha} or p_t^{dis} can be nonzero at any time. To align with Section "Active voltage control problem statement", we use $|p_t^{\text{cha}}|$ and $|p_t^{\text{dis}}|$ as non-negative values, where the non-absolute p_t^{cha} is interpreted as energy consumption with a negative sign. This convention aligns with the BES model, where the energy storage formula is expressed in Eq. (14). Here, p_t^{dis} is the discharging power and p_t^{cha} is the charging power of the BES, respectively; and E_t is the energy stored in the battery at time *t*; Δt denotes the time interval between the previous and the current time step. Finally, the $E^{\max}$ represents the BES's maximum energy capacity, while $E^{\min} = 0$ denotes its minimum and indicates that the BES cannot store negative energy.

$$E_t = E_{t-1} - \left(\eta^{\text{cha}} \cdot p_t^{\text{cha}} + \frac{p_t^{\text{dis}}}{\eta^{\text{dis}}}\right) \cdot \Delta t - \eta^{\text{self}} \cdot E^{\max} \tag{14}$$

where the coefficients η^{dis} and η^{cha} are the discharge and charge efficiencies, and a relative self-discharge rate η^{self} is subject to stochastic uncertainty parameters and models the energy lost at each discrete time steps. This triple of coefficients η^{dis}, η^{cha} and η^{self} is treated as random variables, each following a normal distribution:

$$\eta^{\text{cha}} \sim \mathcal{N}(\mu_c, \sigma_c^2) \tag{15}$$

$$\eta^{\text{dis}} \sim \mathcal{N}(\mu_d, \sigma_d^2) \tag{16}$$

$$\eta^{\text{self}} \sim \mathcal{N}(\mu_s, \sigma_s^2) \tag{17}$$

where μ_c, μ_d, and μ_s are the respective mean values, and σ_c, σ_d, and σ_s denote the corresponding standard deviations. These pairs of variables each define a unique normal distribution. The law of large numbers theorem justifies assumption by ensuring that, given a sufficiently large number of observations, the empirical means and variances converge to their true values, which validates the normal distribution as an approximation. This approach takes into account the nonlinear and uncertain properties of the BES model. It contains typical system noise and measurement errors that are based on the standard deviation of 1%, which is common in PCC voltage metering [28, 60]. This deviation represents a σ of 0.01 μ. It encapsulates both the inherent variability in BES modeling parameters and the probabilistic fluctuations observed in operation, such as the state-of-charge (SoC) and the reachable output power of a BES. Randomly generated normally distributed errors, as represented in the Eqs. (15–17), are estimated with the set of standard deviations $\sigma = [\sigma_c, \sigma_d, \sigma_s] = \{0.01\ \mu_c, 0.01\ \mu_d, 0.01\ \mu_s\}$, fostering a more robust and realistic simulation of system behavior. The BES capacity and efficiency decline over time due to aging effects and a significant rise in internal resistance [39]. As a numerical example, consider a typical lithium-ion BES system with mean charging and discharging efficiencies of $\mu_c = 0.95$ and $\mu_d = 0.95$, and a monthly self-discharge rate of 6–7%. Converted to an hourly rate, this is $\mu_s \approx 0.0001$ (i.e., 0.01% of $E^{\max}$ lost per hour). Over a month or 720 hours, this sums up to $0.0001 \times 720 = 0.072$ or 7.2%. If $E^{\max} = 10\text{kWh}$, the battery will lose 0.001 kWh per hour. These values are consistent with studies on lithium-ion batteries and can be adapted for other battery types or operating conditions [39, 47].

The BES uncertainty parameters, which can be changed or neglected in the configuration file, enable high adaptability when tuning the electrical system model to different use case configurations, and an optional storage scaling factor configured to 1.0 by default. For the operational safety of the electrical grid, maintaining the maximum power limits during charging and discharging is crucial for the operating dynamics of the BES. These operational BES constraints are given in Eqs. (18) and (19), as well as the bus feed-in and feed-out power limitation in Eq. (20).

$$0 \leq -p_t^{\text{cha}} \leq p^{\text{cha}-\max} \tag{18}$$

$$0 \leq p_t^{\text{dis}} \leq p^{\text{dis}-\max} \tag{19}$$

$$p^{\min} \leq p_t^{\text{BUS}} \leq p^{\max} \tag{20}$$

where $p^{\text{cha}-\max}$ and $p^{\text{dis}-\max}$ represent the maximum active power during charging and discharging, and $p^{\min}$ and $p^{\max}$ denote the upper and lower boundaries of bus injection, and p_t^{BUS} represents the net active power exchanged between the grid at the connected bus. The bus feed depends on the load and DER generation and results from the input time series for each time step. The SoC is the ratio of remaining to nominal maximum stored energy:

$$SoC_t = \frac{E_t}{E^{\max}}. \tag{21}$$

The BES's SoC ranges from 0% (fully discharged) to 100% (fully charged). This SoC interval may vary depending on the BES type used and the manufacturer's specifications. Discharging the BES to a SoC below 20% accelerates the degradation [33]. To ensure optimal lifespan and operation, the manufacturer prescribes maintaining an SoC between 20% and 90% [50], which Eq. (22) defines as follows:

$$SoC^{\min} \leq SoC_t \leq SoC^{\max} \tag{22}$$

Finally, Eq. (23) introduces a grid metric associated with line loading:

$$\mathcal{L}_i = \frac{\max(i_{\text{from}}, i_{\text{to}})}{i_{\text{thermal}}^{\max}} \cdot 100 \tag{23}$$

where $\mathcal{L}_i$ denotes the line loading of the distribution line *i*, expressed as a percentage. The line loading is calculated by dividing the maximum current of the connected distribution line *i* by the specified maximum thermal current $i_{\text{thermal}}^{\max}$. This Eq. (23) shows the load on a distribution line relative to its thermal capacity. A line loading near 100 percentages indicates that the line is operating close to its thermal load limit. Values above this can lead to overheating and reduced operating efficiency. This alerts the grid operator to take the necessary action. Figure 3 illustrates the BES modeling chain. It extends from net power input through storage dynamics to SoC and operational constraints.

Monte Carlo methods for electrical grid system simulations

In electrical grid system simulation, MC methods use stochastic parameters to ensure accurate random sampling [5, 37]. These methods are well-suited for modeling

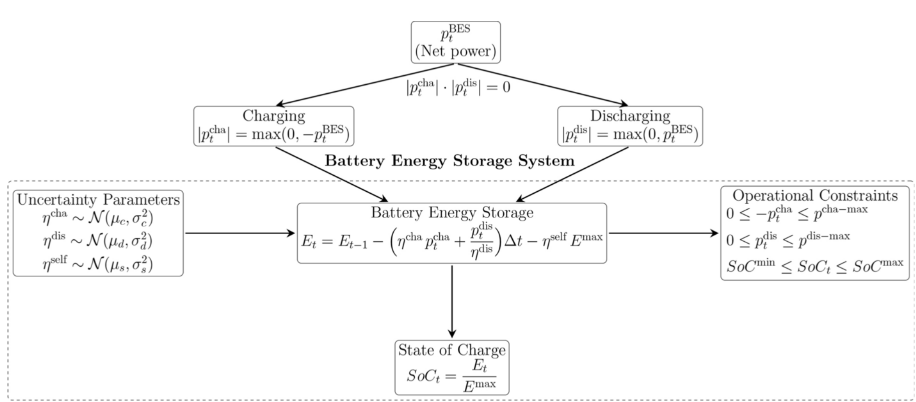

Fig. 3 Illustration of a BES system model with parameter uncertainty and operating constraints

uncertainty in real-world systems, where probabilistic inference is inherently computationally intractable. The most common solution is to approximate results using a finite number of random samples, known as the MC method. MC methods serve two primary purposes: first, to generate random samples from a given probability distribution, and second, to estimate the expected value of a function given a probability distribution with randomly created samples [41]. While a few independent samples can yield reliable estimates [32], increasing the sample size improves accuracy, but also raises computational complexity [10]. MC simulations analyze the robustness and effectiveness of reactive power and grid control strategies under uncertainty. When using MC as a probabilistic method for load flow calculations, stochastic parameters such as the efficiency and self-discharge rates of battery systems can be modeled as normally distributed random variables to capture real-world variability and uncertainties that can occur in practical operations. For each simulation run, the average value of X is calculated over all time steps to obtain a single representative value. Repeating the simulation over multiple runs with different random seeds builds a distribution of outcomes for each metric. This allows for the computation of expected values and variances, providing insights into system behavior under variable conditions. For instance, the expected value of any performance indicator $\mathbb{E}[\mathrm{X}]$ across all runs is given by:

$$\mathbb{E}[\mathrm{X}] = \frac{1}{M}\sum_{j=1}^{M}\left(\frac{1}{N}\sum_{i=1}^{N}\mathrm{X}_{\mathrm{ij}}\right) \tag{24}$$

where M is the number of MC samples, and N is the number of time steps within each power grid simulation. This double-averaging process ensures that each metric reflects the response of the system across dynamic fluctuations, random errors, and other stochastic factors that influence performance. This approach enables a comprehensive sensitivity analysis of reactive power and decision-making control strategies for distributed power generation systems based on inverters.

Influence of the configurable mini photovoltaic rates

Based on several characteristics—α (penetration), β (concentration), γ_1 (configurable apparent peak power) and γ_2 (configurable solar cell power)—we evaluate the impact of MPV on the grid. This analysis follows the PV assessments described in [44]. These configurable parameters can be used to perform a sensitivity analysis of the influence of different configurations of MPV systems on the performance metrics of the LV distribution grid.

α-Characteristic: penetration of mini photovoltaic

For assessing the influence of MPV systems on the LV grid, we introduce MPV penetration rate α, representing a dimensionless ratio between the MPV generation and the consumption of load, defined as:

$$\alpha = \frac{E_{\text{MPV Capacity}}(\gamma_1, \gamma_2, T_{\text{sim}})}{E_{\text{Feeder Capacity}}(T_{\text{sim}})} \tag{25}$$

where $E_{\text{MPV Capacity}}(\gamma_1, \gamma_2, T_{\text{sim}})$ represents the aggregate energy output of MPV systems in the distribution grid over the simulation period T_{sim}, γ_1 describes the configurable apparent peak power of the MPV microinverter, γ_2 represents the configurable solar cell power of the MPV in the configuration file and $E_{\text{Feeder Capacity}}(T_{\text{sim}})$ symbolizes the grid's total energy potential over the simulation period T_{sim}.

β-Characteristic: concentration of mini photovoltaic

Considering the spatial distribution of MPV systems in the electrical grid, we define β as the concentration rate that is expressed by:

$$\beta = \frac{N_{\text{MPV Buses}}}{N_{\text{Load Buses}}} \tag{26}$$

where $N_{\text{MPV Buses}}$ and $N_{\text{Load Buses}}$ denote MPV-attached buses and total load buses, respectively. This β-metric compares the number of MPV systems with the number of loads in the grid. At each load unit, we install one MPVs with concentrations ranging from 0% (indicating no MPV installation) to 100% (indicating one MPV unit at each load unit, resulting in a full MPV concentration level).

Control strategies for distributed energy resources systems

DSOs have traditionally managed voltage regulation through grid reinforcement, including measures by adding lines or modernization of transformers [16]. The grid code described in [60] forms the basis of this Section. DER systems mainly use three local reactive power control modes: *Q*(*V*), *Q*(*P*), and the fixed $\cos\varphi$ mode. These control modes, defined by constant values or piecewise first-order curves, allow DSOs to change these settings remotely, provided they adhere to local DER regulations. Although MPVs are technically usable for voltage regulation, they are not used in this role since VDE regulations do not prescribe reactive power control under 1 kV. It is therefore not considered. To optimize system efficiency, control strategies for PV, BES, and combined PV-BES systems are considered:

1. Decentralized grid control: Each DER unit autonomously makes decisions at the local PCC, independent of grid constraints.
2. Distributed grid control: All DER units along the feeder control zones coordinate the decision-making process jointly.

Reactive power control for distributed energy resources

Before considering each reactive power control scheme, it is important to note that *Q*(*V*), *Q*(*P*) and fixed $\cos\varphi$ each rely on different input signals and operating principles. This leads to varying levels of adaptability to changing grid conditions. In particular, *Q*(*V*) control is highly responsive to local voltage variations. As a result, it is well adapted to feeders with significant voltage fluctuations. In contrast, *Q*(*P*) control matches the reactive power input to the active power output of the DER, which can be advantageous when generation closely matches load demand.

Q(V) control: reactive power-voltage characteristic

The *Q*(*V*) mode primarily addresses the interplay between reactive power and voltage within DER units. Its primary design intent is to oversee and regulate the reactive power interchange between the DER unit and the distribution grid. In this configuration, real-time voltage monitoring takes place at the PCC for each DER unit. To ensure measurement accuracy, the deviation in measurement should not exceed 1% of the *p.u.* value. A foundational dead band around the fixed reference voltage V_{ref}, along with linear Droop control, forms the basis for the $Q(V)$ characteristic:

$$Q(V) = \begin{cases} Q_{\max}, & V \leq V_1 \\ Q_{\max}(1 - \frac{(V-V_1)}{(V_2-V_1)}), & V_1 < V < V_2 \\ 0, & V_2 \leq V \leq V_3 \\ -Q_{\max}\frac{(V-V_3)}{(V_4-V_3)}, & V_3 < V < V_4 \\ -Q_{\max}, & V \geq V_4 \end{cases} \tag{27}$$

Parameters V_1, V_2, V_3, and V_4 in this piecewise function are adjustable based on DSO conditions and set the voltage deadband limits.

Q(P) control: active power-power factor characteristic

The $Q(P)$ mode primarily targets the direct adjustment of the DER unit's reactive power in response to its momentary active power generation. Commonly known as the Power Factor (PF), this relationship is symbolized by $\cos\varphi$. It represents the cosine value of the phase difference existing between active and apparent power. When the measured active power actual value P_{AV} exceeds the threshold P_1, a linear transition in $\cos\varphi(P_{\mathrm{AV}})$ ensues, shifting from a predefined PF value C_1 to C_2. The characteristic is illustrated as follows:

$$\cos\varphi(P) = \begin{cases} C_1, & P < P_1 \\ C_1 + (P - P_1)\frac{(C_2-C_1)}{(P_2-P_1)}, & P_1 \leq P \leq P_2 \\ C_2, & P > P_2 \end{cases} \tag{28}$$

In mathematical terms, the reactive power can be represented as:

$$Q(P) = P \cdot \tan(\arccos\varphi(P)) \tag{29}$$

This formulation captures the dynamic interplay of reactive power $Q(P)$ and the real-time active power value P_{AV}, using the PF characteristic $\cos\varphi(P)$ from Eq. (28).

Fixed $\cos\varphi$ control: constant power factor characteristic

In contrast to methods with feedback control mechanisms, the fixed ratio of active to reactive power in $\cos\varphi = \mathrm{const}$ mode remains unchanged. In this mode, the reactive power from the DER, as depicted in Eq. (29), correlates directly with its active power, starting from a threshold value of P_1. The grid operator sets the factor $\cos\varphi$ in accordance with the grid code and the permissible range of the DER unit.

Control strategies for distributed energy resources

We evaluate control strategies for PV, BES and combined PV-BES in the PCC. Table 1 provides an overview of the DER control strategies applied in LV grids. In this work, we do not apply these control strategies to MPVs. Active voltage control of PV inverters is adjusted according to the VDE grid code based on the PCC voltage measurement or the actual PV power output. To implement the distributed control strategy, the Dijkstra pathfinding algorithm is used to identify the main branch of each grid, partitioning it into control zones between the feeder and the transformer substation. This approach aligns with the German Energy Industry Act [24], which mandates non-discriminatory

Table 1 Overview of DER control strategies

Strategies	Description	Approach
PV strategy 1	Powers local consumption P_t^{Load}	Decentralized
	Feeds residual power P_t^{RES} into the grid	
BES strategy 1	Charges BES to $SoC^{\max}$ from 6:00 a.m. to 6:00 p.m.	Decentralized
	Discharges BES to $SoC^{\min}$ from 6:00 p.m. to 6:00 a.m.	
PV-BES strategy 1	Charges BES if residual local power ($P_t^{\mathrm{RES}} > 0$)	Distributed
	Discharges BES if residual local power ($P_t^{\mathrm{RES}} < 0$)	
PV-BES strategy 2	Each operator manages a control zone within LV grid	Distributed
	Calculates joint zone residual power $P_{t,\mathrm{zone}}^{\mathrm{RES}}$	
	Charges BES with residual power if ($P_{t,\mathrm{zone}}^{\mathrm{RES}} > 0$)	
	Discharges BES with residual power if ($P_{t,\mathrm{zone}}^{\mathrm{RES}} < 0$)	
	Grid supply if ($P_{t,\mathrm{zone}}^{\mathrm{RES}} > 0$) and $SoC_{t,zone} = SoC^{\max}$	
	BES idle mode if no charging or discharging is required	
PV-BES strategy 3	Charges BES during DNC periods if ($P_{t,\mathrm{zone}}^{\mathrm{RES}} > 0$)	Distributed
	Discharges BES during DNC periods if ($P_{t,\mathrm{zone}}^{\mathrm{RES}} < 0$)	

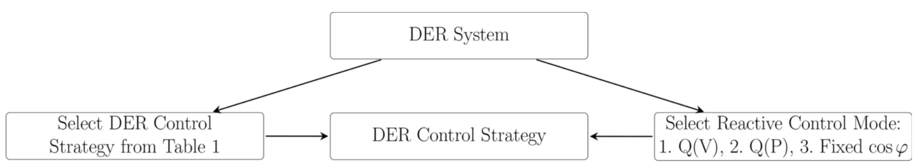

Fig. 4 Decision workflow for DER control, including strategy selection and reactive power control modes

grid access for all operators. Some feeder zones contain multiple diverse DERs, whereas others have none, reflecting realistic grid conditions. Cost savings in this study derive from minimizing total active losses, assuming a constant electricity price. Minimization includes factors such as reactive power generation and grid losses. Although each DER operates under decentralized ownership, the distributed control approach allows multiple owners to collaborate within a feeder zone. In the distributed control system, the feeder control zones, which extend from the substation to the end of the feeder, are equipped with communication devices. These devices can exchange information and make dynamic decisions on the feed-in or feed-out of power to the grid. Figure 4 represents the decision workflow for selecting a DER control strategy from Table 1. In addition, it selects one of the three reactive power control modes described in Sections "Q(V) control: reactive power-voltage characteristic", "Q(P) control: active power-power factor characteristic", and "Fixed cos ϕ control: constant power factor characteristic".

Experimental settings

This section describes the experimental settings of three case studies on a 15-bus electrical grid. Case study 1 performs a sensitivity analysis over 366 days (35136 time steps) with a smaller number of MC samples (M=20) to gain initial insights. A larger number is not feasible due to computational limitations. With a simulation horizon of one year and 60 parameter combinations, conducting more than 20 MC samples corresponds to 1,200 one-year simulation runs. However, these M=20 samples are sufficient to give a first indication on the influence of the integration of MPV systems of α, β, γ_1, and γ_2 on grid performance. Case studies 2 and 3 use more MC samples (M=100), resulting in statistically more robust estimates. These larger MC samples confirm the trends from case study 1, thus testing the validity of our assumptions. The second case study compares different reactive power control methods over one day (96 time steps). The distributed control strategy (PV-BES strategy 2) remains fixed while the grid's response to different reactive power control modes is analyzed. The third case study compares decentralized and distributed grid control strategies over 24 hours with 96 time steps. The $Q(V)$ is fixed in this case. We focus on analyzing the charging and discharging processes of BES, the SoC of BES, and the grid limitation on the distribution lines. Each simulation starts with random initial values set in the configuration file, with a resolution of $\Delta t = 15$ min per step.

Benchmarks

To evaluate the control mechanisms in inverter-based DER, we use the benchmark tool SimBench [36], which provides load and PV profiles as well as electrical grid topologies for simulation. This tool provides an open-source, measurement-based set of grid topologies, including all technical constraints and installed components. It also offers representative load and generation time series at different voltage levels. These realistic profiles capture the inherent variability of real-world demand and renewable generation more accurately than standardized or synthetic data. Integrating the widely used SimBench models [36] into our simulations ensures that our control strategies are evaluated under realistic operating conditions. Consequently, this improves the reliability and relevance of our results. We partition the feeder control regions described in Section "Control strategies for distributed energy resources" and integrate them into the grid topology information. Additional MPVs units can be added to the electrical grid with a configurable MPV concentration, as described in Section "Influence of the configurable mini photovoltaic rates". In the general approach for all grid topologies described, we extend each BES bus with solar power plants, leading to a PV-BES system. Specifically, in the case studies of the 15-bus electrical grid, this extension involves adding five solar power plants at buses 6, 9, 10, 12, and 14, as depicted in Fig. 5. The numbers in black represent

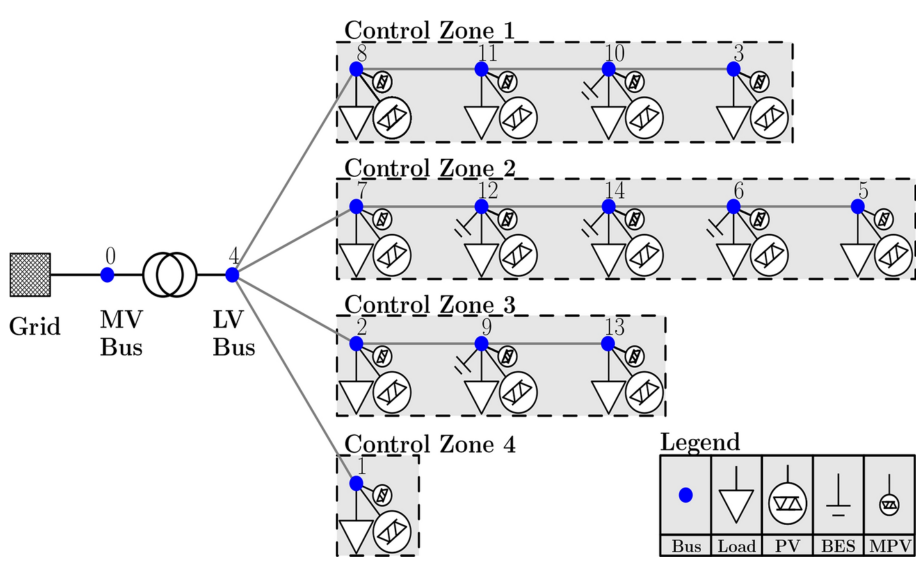

Fig. 5 15-bus LV distribution grid segmented into four feeder control zones extending from the feeder end-terminal to the substation. Blue circles mark each bus. Buses 0–4 indicate the main connections between the substation and the external grid

the bus indexes. The grid consists of 15 buses, 13 lines, 1 transformer, 5 BES, and 13 PV systems, with bus 0 acting as a slack bus. The number of MPVs varies depending on the configuration parameters. The initial state SoC of all BES on buses 6, 9, 10, 12, 14 is 0%.

Load and photovoltaic profiles

In our simulation, load, PV and MPV power data are added with truncated Gaussian noise, representing noisy measurements. The standard deviations of this noise are set to $\sigma_{\text{noise}} = [\sigma_{\text{noise}}^{\text{Load}}, \sigma_{\text{noise}}^{\text{PV}}, \sigma_{\text{noise}}^{\text{MPV}}] = [10^2, 10, 10]$ in p.u. and correspond to the respective data of the grid elements. The PV profile has a $\cos\varphi$ magnitude of 1.0.

Mini photovoltaic profiles

Two regions in Germany, the urban district of Pforzheim and the rural district of Karlsruhe in the federal state of Baden-Württemberg have different zonal solar radiation characteristics. Smart plugs record the output data of MPV units in real-time as MPV profiles. A total of six MPVs are paired at three different locations, with two MPVs at each location ensuring spatial-geometric correlation. For the case studies, the MPV units in the same control zone have the same PV profiles from the benchmark as they are geometrically correlated. Each load is randomly assigned an MPV unit in the control zones within the electrical grid, and the MPV profiles are also randomly assigned.

Performance metrics

The integration of MPV as a renewable energy source into the generation portfolio can cause additional stress on the electrical distribution grids. Most renewable energy sources are connected to the grid via inverters, which must be technically capable of supplying reactive power. In practice, MPVs can provide reactive power, but this function is not taken into account by the regulatory framework. Considering the inherent limitations of distribution lines, such as non-negligible resistances and limited transmission capacities, overload problems, including the number of violations of overload limits, the average overload of lines and transformers, voltage magnitudes, aggregate reactive power injection from DER inverters and power losses, can be used to evaluate grid control methods [15, 20, 38]. We introduce four different performance metrics to evaluate the case studies of our proposed inverter control strategies:

- **Voltage Magnitude VM:** This metric calculates the average VM across all buses for each simulation step, expressed in p.u.
- **Grid Loss (GL):** This metric calculates the total losses of lines and transformers across all buses for each simulation step. The GL are aggregated over time in MW.
- **Transformer Loading (TL):** This metric calculates the average TL for each time step during a simulation and represents the load utilization in relation to the rated power as a percentage.
- **Line Loading (LL):** This metric calculates the average LL per time step during a simulation.By evaluating these metrics, one could anticipate potential reductions in grid losses and alleviation of stress on system components and ensure cost savings.

Results and discussion

Case study 1: sensitivity analysis of mini photovoltaic integration

In the first case study, we analyze the sensitivity considering the parameters α, β, γ_1, and γ_2, as shown in Fig. 6. In this case, we only use the distributed grid control strategy with the PV-BES strategy 3 from Table 1 and the reactive power control $Q(V)$ from Section "Reactive power control for distributed energy resources". This sensitivity analysis addresses how the integration of MPV influences the electrical grid depending on the parameterization, particularly regarding the penetration and concentration of MPV as well as the configurable peak and solar cell power. As indicated in the legend, the blue dashed line with the triangular marker represents the configurable apparent power peak (γ_1) for 600 VA; the orange dashed line with the square marker for 800 VA and the green dotted-dashed lines with the diamond marker for 1000 VA. The horizontal axis represents the concentration level of the MPV, β, in percentage, while the vertical axis shows the respective key performance metrics according to their corresponding units. The sub-figures represent the solar cell capacity parameter γ_2 for (a) 800 W, (b) 1200 W, (c) 1600 W and (d) 2000 W. The results show that the average VM for $\gamma_2 = 1200$ shows a piecewise linear increase with increasing β. This phenomenon can be attributed to the reactive power control of DER systems. The analysis shows that both the TL, which varies from an average of 30% to 33.5% and the LL, which increases from 39.5% to 42.5%, follow a piecewise linear function in response to increasing parameter values of β and γ_2. Due to the pure active power feed-in of the MPV, the integration significantly increases the active power injection at the PCC. To sum up, the sensitivity analysis shows that DERs counteract this with reactive power control to keep the voltages within limits. As a result, the integration of the MPV leads to an increase in the reactive power provision and inverter losses. In addition, more reactive power leads to higher inverter losses [14]. This study neglects deviations in active power loss between inverters

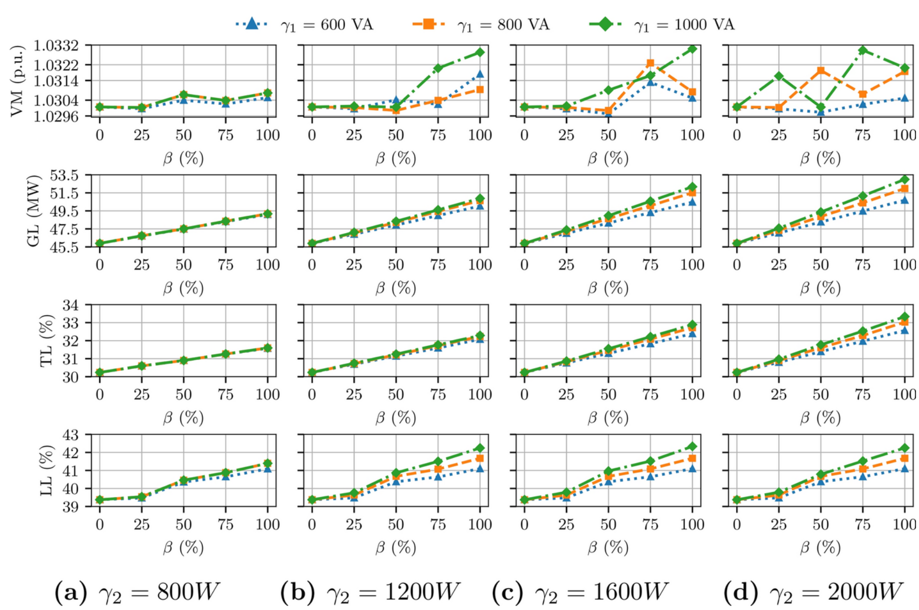

Fig. 6 Sensitivity analysis with (M = 20) MC samples over one-year power flow calculations illustrates the impact of MPV concentrations in LV grids using four solar cell capacities: subfigures (**a**) 800 W, (**b**) 1200 W, (**c**) 1600 W, and (**d**) 2000 W. Each subfigure shows the relationship between the MPV concentration rates and performance metrics for three MPV inverter apparent power levels: 600 VA, 800 VA, and 1000 VA

due to different PF settings. This use case covers *RQ1* by analyzing the impact of increasing MPV penetration on grid stability and reverse power flow in radial LV grids. It also analyses the influence of key parameters on the voltage increase for operational efficiency and grid security, directly addressing *RQ2*. As shown in Figure 6, the grid stability metrics (LL, TL, and VM) increase linearly with increasing MPV integration. In summary, when MPV penetration exceeds 75%, GL increases significantly. Consequently, the reactive power control $Q(V)$ compensates for the voltage rise at the PCC by providing additional reactive power to maintain voltage stability.

Case study 2: comparison of reactive power control modes

In this extended case study, we analyze the performance of different reactive power control modes in the distribution grid, considering the uncertainty by employing 100 MC runs while keeping a consistent distributed control strategy (PV-BES strategy 2). Our environment evaluates different voltage regulation modes, as shown in Fig. 7. The four methods analyzed are as follows: $Q(V)$, represented by a solid blue line; $Q(P)$, depicted as a dashed orange line; Fixed $\cos\varphi$ control, shown with a green dashed line; and no control with a red dotted line. The first row shows the average VM across all MC simulations, while the second the reactive power feed-in of the PV systems. Each method controls the voltage within the safety range, despite 100% MPV concentration levels. In addition, the VM values of $Q(V)$ are below those of the $\mathrm{Fixed}\cos\varphi$ control but above those of $\cos\varphi$. This behavior occurs because $\mathrm{Fixed}\cos\varphi$ operates with a constant PF,

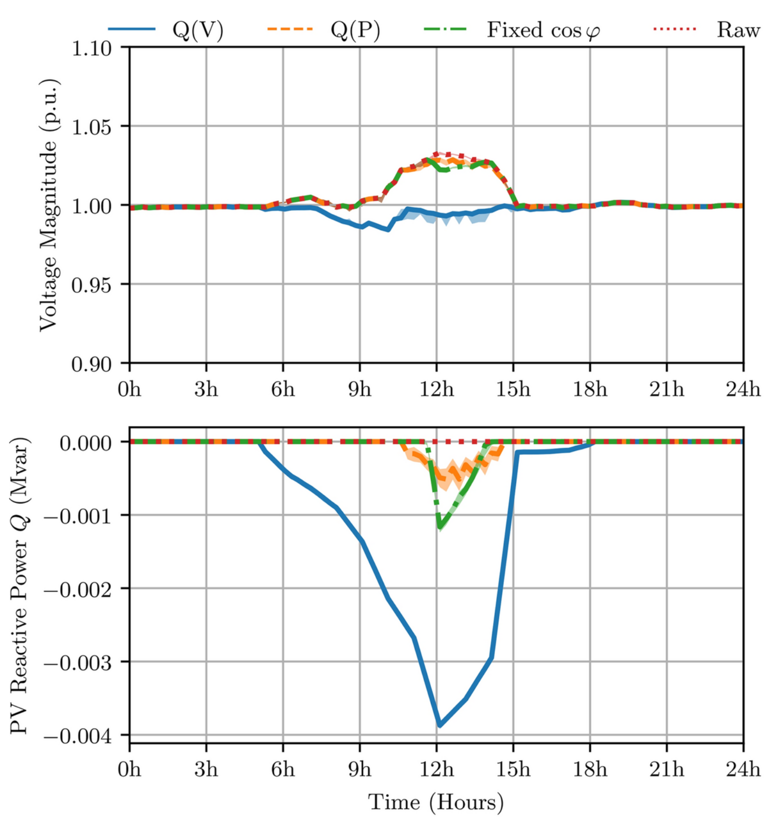

Fig. 7 Case study 2–reactive power and voltage variations under different control methods, shown over $M = 100$ Monte Carlo samples on a summer day. Shaded areas indicate the 99% confidence interval around the mean values

unable to dynamically reduce reactive power injection. In contrast, $\cos\varphi$ injects the reactive power based on a threshold value of the active power, whereas $Q(V)$ activates the reactive power only when the voltage exceeds the regulatory threshold, leading to a characteristic zigzag pattern in VM. Using $Q(V)$ significantly improves MPV integration in inverter-based DERs, reducing active power curtailment and optimizing grid performance. This case study directly addresses *RQ3* by comparing multiple inverter control strategies. The goal is to assess their effectiveness in optimizing self-consumption and ensuring grid stability. The results indicate that all modes keep the voltage within safety limits, even under 100% MPV concentration. Such outcomes highlight the crucial role of dynamic reactive power control in enhancing grid performance. Additionally, Fig. 7 demonstrates that $Q(P)$ exhibits the lowest power dissipation, with fixed $\cos\varphi$ and $Q(V)$ following in that order.

Case study 3: comparison of decentralized and distributed grid control strategies

This third case study evaluates decentralized versus distributed grid control strategies, as shown in Table 1. For all strategies, $Q(V)$ was selected as the reactive power control mode. Figure 8 shows the charging and discharging process of the power in the first row, the SoC of the respective BES in the second row and the average LL of the distribution lines in the third row. Shaded areas indicate the 99% confidence interval around the mean values. The sub-figures represent (a) PV-BES strategy 1, (b) strategy 2, and (c) strategy 3. High solar power generation in the grid leads to a high average load on the lines (LL). In addition, the LL increases when the BES are actively charging and discharging. At distributed control strategy 3, this becomes clear between 6:00 p.m. and midnight, when the BES units are discharging. Under the decentralized approach, the LL also increases during the charging processes from 6 a.m. to 12 p.m. The five BES units of the distributed PV-BES strategy 2 charges almost fully between in the same period. It is important to note that all BES units follow the same control algorithm. However, differences in battery capacity and local load consumption result in distinct SoC trajectories. For instance, the BES on Bus 9 exhibits a smaller capacity. Consequently, this unit reaches higher SoC values more quickly. Its small capacity leads to a moderate increase in LL. In contrast, other BES units with larger capacities exhibit slower charging and discharging rates. Due to the limitations of SoC between 20% and 90%, it is not feasible to charge above 86% or discharge below 24%. Distributed Day-Night-Control (DNC) starts charging all BES at 6 a.m., based on the charging timestep setting. In contrast, with the decentralized approach and distributed strategy 2, only one BES is fully charged during this period, while the other BES units reach a lower SoC. The DNC begins to discharge fully at 6 p.m., causing a high LL. As a result, other PV surplus energy actively transfers to the higher-level grid through the slack bus. However, distributed control strategies enable faster charging as they can exchange access to PV power in the feeder control zone. The distributed control system stores energy to compensate for future load peaks, while the decentralized control only covers local demand. This case study responds to *RQ3* by determining whether decentralized or distributed control strategies are more effective in integrating MPVs. Distributed grid control manages the BES more effectively than the decentralized approach. However, the latter regulates the voltage over a smaller range than the distributed control. This is due to the fact that PV systems and the BES operate independently within the distribution grid.

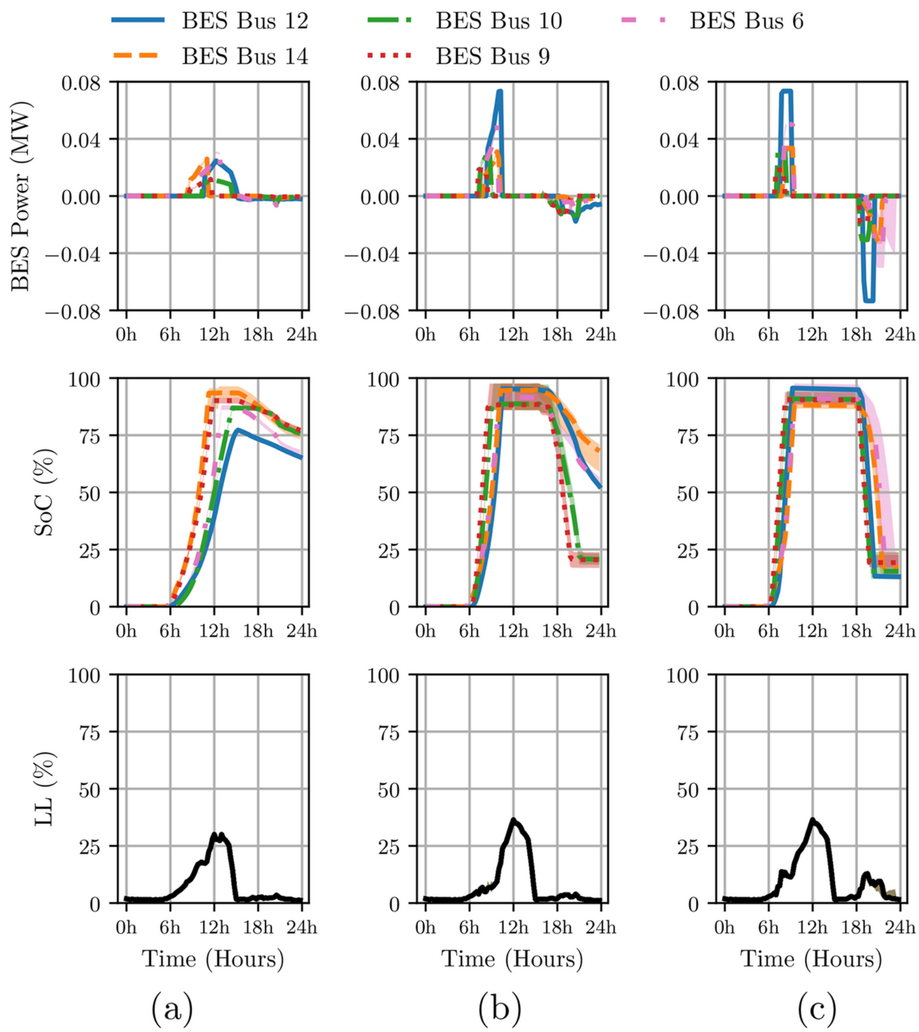

Fig. 8 Case Study 3–Results averaged over $M = 100$ Monte Carlo samples. Top sub-figures: BES charging/discharging under PV-BES Strategies (**a**) 1, (**b**) 2, and (**c**) 3. Middle: Daily SoC status. Bottom: Average LL status

Conclusion

The present paper provides a comprehensive MC analysis of MPV systems, commonly known as balcony power plants, and their impact on the stability and control of the LV grid. Increasing the penetration of MPV and the inverter power leads to raising the transformer load by up to 3%, raises the line load by 2.5% and maintaining the voltage magnitude through reactive power control, resulting in a power loss of about 17%. These case studies highlight the essential role of autonomous inverters in providing ancillary services in DER-rich grids and underscore the need for adaptable DER control strategies. Our analysis shows that increased MPV penetration significantly impacts grid stability, as demonstrated by the occurrence of reverse power flows and higher transformer loads. The observed voltage rises under high MPV levels are effectively managed by reactive power control but at the cost of increased inverter losses. Comparative evaluations confirm that dynamic inverter control strategies improve self-consumption and overall grid efficiency compared to static approaches. In addition, distributed grid management proves more effective than decentralized methods in coordinating energy storage and absorbing local power peaks. These findings underscore the need for adaptive regulatory frameworks to support the growing integration of MPV and DER in modern distribution grids. The MPVBench dataset is based on real measurements from balcony power plants and covers data from 2024. In addition, we publish PIDE, an open-source Python framework that provides a comprehensive platform for researching and developing reactive power and grid control strategies that are compliant with grid codes. It enables researchers to simulate the integration and impact of DER, such as balcony power plants, while offering reference solutions for voltage regulation and DER control aligned with grid codes to support future applied energy research. Although PIDE provides deeper analysis and control of solar power generation and batteries, it does not consider heterogeneous DERs (e.g., electric vehicles, heat pumps) or dynamic energy price signals. To fill these gaps, our future research will focus on integrating additional DER components alongside dynamic energy price signals. We will also investigate advanced algorithms, including single- and multi-objective RL, to simultaneously optimize conflicting objectives such as grid stability and economic optimization. Our primary research focus remains the application of AI and RL to grid control for DERs.

Author Contributions

GD led the conceptual development, implementation and paper writing. NF and SG contributed to review and editing. KF and VH were responsible for funding acquisition, supervision, review and editing. All authors read and approved the final manuscript.

Funding

Open Access funding enabled and organized by Projekt DEAL. This work was supported in part by the Energy System Design (ESD) Project within the structure 37.12.02; in part by the Helmholtz Association (HGF) Initiative and Networking Fund through Helmholtz AI and the HAICORE@KIT partition.

Data Availability

The MPVBench dataset [18] is available at https://github.com/KIT-IAI/MPVBench and has been extended to cover the full year of 2024. The open-source framework PIDE is available on GitHub: https://github.com/KIT-IAI/PIDE.

Declarations

Ethics approval and consent to participate

Not applicable.

Consent for publication

Not applicable.

Competing interests

The authors declare that they have no competing interests.

Received: 18 January 2025 / Accepted: 17 February 2025

Published online: 04 March 2025

References

1. Agalgaonkar YP, Pal BC, Jabr RA (2014) Distribution voltage control considering the impact of PV generation on tap changers and autonomous regulators. IEEE Transactions on Power Systems 29(1):182–192. https://doi.org/10.1109/tpwrs.2013.2279721
2. Akinyemi AS, Musasa K, Davidson IE (2022) Analysis of voltage rise phenomena in electrical power network with high concentration of renewable distributed generations. Scientific Reports 12(1):1–22. https://doi.org/10.1038/s41598-022-11765-w
3. von Appen J, Stetz T, Braun M et al (2014) Local voltage control strategies for PV storage systems in distribution grids. IEEE Transactions on Smart Grid 5(2):1002–1009. https://doi.org/10.1109/TSG.2013.2291116
4. Ari G, Baghzouz Y (2011) Impact of high PV penetration on voltage regulation in electrical distribution systems. In: International Conference on Clean Electrical Power (ICCEP). IEEE, Ischia, pp 744–748, https://doi.org/10.1109/ICCEP.2011.6036386
5. Atzberger PJ (2006) The Monte-Carlo Method. https://web.math.ucsb.edu/~atzberg/pmwiki_intranet/uploads/AtzbergerHomePage/Atzberger_MonteCarlo.pdf, https://api.semanticscholar.org/CorpusID:5339065, doi, Retrieved Dec. 17, 2024
6. Baran M, Wu F (1989) Network reconfiguration in distribution systems for loss reduction and load balancing. IEEE Transactions on Power Delivery 4(2):1401–1407. https://doi.org/10.1109/61.25627
7. Baran M, Wu F (1989) Optimal sizing of capacitors placed on a radial distribution system. IEEE Transactions on Power Delivery 4(1):735–743. https://doi.org/10.1109/61.19266
8. Bergner J, Hoelger R, Praetorius B (2022) The Market for Plug-In Solar Devices. Tech. Rep. 1, Hochschule für Technik und Wirtschaft HTW Berlin, https://solar.htw-berlin.de/studien/marktstudie-steckersolar-2022

9. Biel D, Scherpen JM (2018) Active and reactive power regulation in single-phase PV inverters. In: 2018 European Control Conference (ECC). IEEE, https://doi.org/10.23919/ECC.2018.8550507
10. Bishop C (2007) Pattern Recognition and Machine Learning (Information Science and Statistics). Springer
11. BMWK (2023) Photovoltaic Strategy: Fields of Action and Measures for an Accelerated Expansion of Photovoltaics. Bundesministerium für Wirtschaft und Klimaschutz (BMWK) 1:1–42. https://www.bmwk.de/Redaktion/DE/Publikationen/Energie/photovoltaik-stategie-2023
12. BNetzA (2024) Archived EEG feed-in tariffs. Quarterly reported new installations of PV systems and current feed-in tariffs of the German Renewable Energy Act. Bundesnetzagentur (BNetzA). Archived from the https://web.archive.org/web/20240202124405/https://www.bundesnetzagentur.de/DE/Fachthemen/ElektrizitaetundGas/ErneuerbareEnergien/EEG_Foerderung/Archiv_VergSaetze/start.html original on Jan. 2024. Retrieved Dec. 17, 2024
13. BNetzA MaStR (2024) Public Unit Overview in the German Market Master Data Register: Solar Energy Units with a Gross Power Output Below 1 kW. German Market Master Data Register (MaStR). https://www.marktstammdatenregister.de/MaStR/Einheit/Einheiten/OeffentlicheEinheitenuebersicht?filter=Bruttoleistung%20der%20Einheit%7Elt%7E%271%27%7Eand%7EEnergietr%C3%A4ger%7Eeq%7E%272495%27%7Eand%7EBetriebs-Status%7Eeq%7E%2735%27%7Eand%7ENettonennleistung%20der%20Einheit%7Elt%7E%271%27. Retrieved Dec. 17, 2024
14. Braun M, Stetz T, Reimann T et al (2009) Optimal Reactive Power Supply in Distribution Networks - Technological and Economic Assessment for PV Systems. In: Proceedings of the 24th European Photovoltaic Solar Energy Conference (EU PVSEC 2009), Hamburg, Germany
15. Brown RE (2008) Impact of smart grid on distribution system design. In: (2008) IEEE Power and Energy Society General Meeting-Conversion and Delivery of Electrical Energy in the 21st Century. IEEE. https://doi.org/10.1109/pes.2008.4596843
16. Carvalho P, Correia P, Ferreira L (2008) Distributed reactive power generation control for voltage rise mitigation in distribution networks. IEEE Transactions on Power Systems 23(2):766–772. https://doi.org/10.1109/TPWRS.2008.919203
17. CENELEC (2022) German Institute for Standardisation Registered Association (DIN) and European Committee for Electrotechnical Standardization (CENELEC), DIN EN 50160:2022-10, Voltage characteristics of electricity supplied by public distribution networks. DIN Standards 2(1):1–116. https://dx.doi.org/10.31030/3383427
18. Demirel G, Grafenhorst S, Förderer K et al (2025) Impact and integration of mini photovoltaic systems on electric power distribution grids. In: Jørgensen BN, Ma ZG, Wijaya FD et al (eds) Energy Informatics. Springer Nature Switzerland, Cham, pp 247–265
19. Demirok E, González PC, Frederiksen KHB et al (2011) Local reactive power control methods for overvoltage prevention of distributed solar inverters in low-voltage grids. IEEE Journal of Photovoltaics 1(2):174–182. https://doi.org/10.1109/JPHOTOV.2011.2174821
20. Dorfler F, Bolognani S, Simpson-Porco JW, et al (2019) Distributed control and optimization for autonomous power grids. In: 2019 18th European Control Conference (ECC). IEEE, https://doi.org/10.23919/ecc.2019.8795974
21. DSIRE (2024) Net metering policies. https://www.dsireusa.org/resources/detailed-summary-maps/net-metering-policies-2/, Database of State Incentives for Renewables and Efficiency (DSIRE), North Carolina Clean Energy Technology Center (NCCETC). Accessed: Dec. 17, 2024
22. EC (2016) European Commission (EC) Commission Regulation (EU) 2016/631 of 14 Apr. 2016 establishing a network code on requirements for grid connection of generators. Official Journal of the European Union 1(631):1–68. http://data.europa.eu/eli/reg/2016/631/oj
23. Energy Networks Association (2022) Engineering Recommendation G99, Issue 1 - Amendment 9. Published by Energy Networks Association, London (UK), 3 October 2022, https://www.energynetworks.org
24. EnWG (2024) Act on the supply of electricity and gas (energy industry act - enwg). https://www.gesetze-im-internet.de date of issue: 07.07.2005. Full citation: "Energy Industry Act of 7 July 2005 (BGBl. I p. 1970; corrected p. 3621), in force since 13.07.2005, as last amended by the Act of 14 May 2024 (BGBl. I p. 161) effective as of 17.05.2024 and 01.06.2024 respectively". Status: As of 01.07.2024
25. Farivar M, Low SH (2013) Branch flow model: Relaxations and convexification—part i. IEEE Transactions on Power Systems 28(3):2554–2564. https://doi.org/10.1109/TPWRS.2013.2255317
26. Gautier A, Jacqmin J, Poudou JC (2018) The prosumers and the grid. Journal of Regulatory Economics 53(1):100–126. https://doi.org/10.1007/s11149-018-9350-5
27. Geth F, Tant J, Haesen E, et al (2010) Integration of energy storage in distribution grids. In: IEEE PES General Meeting. IEEE, Minneapolis, pp 1–6, https://doi.org/10.1109/PES.2010.5590082
28. IEEE (2018) IEEE Standard for Interconnection and Interoperability of Distributed Energy Resources with Associated Electric Power Systems Interfaces. IEEE Std 1547-2018 (Revision of IEEE Std 1547-2003) 2(1):1–138. https://doi.org/10.1109/IEEESTD.2018.8332112
29. Ju Y, Zhang Z, Wu W et al (2022) A bi-level consensus admm-based fully distributed inverter-based volt/var control method for active distribution networks. IEEE Transactions on Power Systems 37(1):476–487. https://doi.org/10.1109/tpwrs.2021.3097798
30. Kabir MN, Mishra Y, Ledwich G et al (2014) Coordinated control of grid-connected photovoltaic reactive power and battery energy storage systems to improve the voltage profile of a residential distribution feeder. IEEE Transactions on Industrial Informatics 10(2):967–977. https://doi.org/10.1109/TII.2014.2299336
31. Kerber G, Witzmann R, Sappl H (2009) Voltage limitation by autonomous reactive power control of grid connected photovoltaic inverters. In: 2009 Compatibility and Power Electronics. IEEE, Badajoz, pp 129–133, https://doi.org/10.1109/CPE.2009.5156024
32. MacKay DJC (2002) Information Theory. Inference and Learning Algorithms,Cambridge University Press, USA,
33. Marra F, Yang G, Traeholt C et al (2014) A decentralized storage strategy for residential feeders with photovoltaics. IEEE Transactions on Smart Grid 5(2):974–981. https://doi.org/10.1109/TSG.2013.2281175
34. Masters C (2002) Voltage rise: the big issue when connecting embedded generation to long 11 kV overhead lines. Power Engineering Journal 16(1):5–12. https://doi.org/10.1049/pe:20020101
35. Matkar G, Dheer DK, Vijay AS, et al (2017) A simple mathematical approach to assess the impact of solar PV penetration on voltage profile of distribution network. In: National Power Electronics Conference (NPEC). IEEE, Pune, pp 209–214, https://doi.org/10.1109/NPEC.2017.8310460

36. Meinecke S, Sarajlić D, Drauz SR et al (2020) SimBench—a benchmark dataset of electric power systems to compare innovative solutions based on power flow analysis. Energies 13(12):3290. https://doi.org/10.3390/en13123290
37. Metropolis N, Ulam S (1949) TThe Monte Carlo Method. Journal of the American Statistical Association 44(247):335–341. http://www.jstor.org/stable/2280232
38. Mueller F, de Jongh S, Mu X, (2023) Sector-coupled distribution grid analysis for centralized and decentralized energy optimization. In, et al (2023) 58th International Universities Power Engineering Conference (UPEC). IEEE. https://doi.org/10.1109/UPEC57427.2023.10294701
39. Naumann M, Karl RC, Truong CN et al (2015) Lithium-ion Battery Cost Analysis in PV-household Application. Energy Procedia 73:37–47. https://doi.org/10.1016/j.egypro.2015.07.555, 9th International Renewable Energy Storage Conference, IRES 2015
40. Omran WA, Kazerani M, Salama MMA (2011) Investigation of methods for reduction of power fluctuations generated from large grid-connected photovoltaic systems. IEEE Transactions on Energy Conversion 26(1):318–327. https://doi.org/10.1109/TEC.2010.2062515
41. Park J, Karumanchi S, Iagnemma K (2015) Homotopy-based divide-and-conquer strategy for optimal trajectory planning via mixed-integer programming. IEEE Transactions on Robotics 31(5):1101–1115. https://doi.org/10.1109/TRO.2015.2459373
42. Poullikkas A, Kourtis G, Hadjipaschalis I (2013) A review of net metering mechanism for electricity renewable energy sources. International Journal of Energy and Environment 4:975–1002. https://www.ijee.ieefoundation.org/vol4/issue6/IJE E_06_v4n6.pdfdoi, Retrieved Dec. 17, 2024
43. Qu G, Li N (2020) Optimal distributed feedback voltage control under limited reactive power. IEEE Transactions on Power Systems 35(1):315–331. https://doi.org/10.1109/tpwrs.2019.2931685
44. Quezada V, Abbad J, Roman T (2006) Assessment of energy distribution losses for increasing penetration of distributed generation. IEEE Transactions on Power Systems 21(2):533–540. https://doi.org/10.1109/TPWRS.2006.873115
45. Rostami SM, Hamzeh M, Nazaripouya H (2024) Distributed Cooperative Reactive Power Control of PV Systems With Dynamic Leader. IEEE Transactions on Industrial Informatics 20(6):8972–8982. https://doi.org/10.1109/tii.2024.3372615
46. Roth A, Kühlmeyer H, Nollau A, et al (2023) Plug-and-Play Mini Power Generation Plants. VDE Position Papers, https://www.vde.com/resource/blob/2229846/acbd1078371f6a553a049a1d33b8612c/positionspapier-data.pdf, dec. 17, 2024
47. Schmidt JP, Weber A, Ivers-Tiffée E (2015) A novel and fast method of characterizing the self-discharge behavior of lithium-ion cells using a pulse-measurement technique. Journal of Power Sources 274:1231–1238. https://doi.org/10.1016/j.jpowsour.2014.10.163
48. Schmitz A, Ofenheusle C, Müller S, et al (2024) Balkonkraftwerke für alle: Der Leitfaden für die Energiewende zum Selbermachen [Balcony Power Plants for Everyone: The DIY Guide to the Energy Transition]. Self-published, https://www.akkudoktor.net/balkonsolar-buch/
49. Singh NK, Elrayyah A, Wanik MZC (2020) Analysis of voltage rise and optimal PV curtailment strategy for its mitigation. In: 2020 IEEE PES Innovative Smart Grid Technologies Europe (ISGT-Europe). IEEE, The Hague, pp 610–614, https://doi.org/10.1109/ISGT-Europe47291.2020.9248971
50. SMA Solar Technology (2023) SMA SMART HOME: Battery Charging Management with Time-of-Use Energy Tariffs. Niestetal, Deutschland, www.sma.de
51. Stetz T, Marten F, Braun M (2013) Improved Low Voltage Grid-Integration of Photovoltaic Systems in Germany. IEEE Transactions on Sustainable Energy 4(2):534–542. https://doi.org/10.1109/TSTE.2012.2198925
52. Stetz T, Diwold K, Kraiczy M et al (2014) Techno-economic assessment of voltage control strategies in low voltage grids. IEEE Transactions on Smart Grid 5(4):2125–2132. https://doi.org/10.1109/TSG.2014.2320813
53. Stetz T, von Appen J, Niedermeyer F et al (2015) Twilight of the Grids: The Impact of Distributed Solar on Germanys Energy Transition. IEEE Power and Energy Magazine 13(2):50–61. https://doi.org/10.1109/MPE.2014.2379971
54. Subhonmesh B, Low SH, Chandy KM (2012) Equivalence of branch flow and bus injection models. In: 2012 50th Annual Allerton Conference on Communication, Control, and Computing (Allerton). IEEE, Monticello, pp 1893–1899, https://doi.org/10.1109/Allerton.2012.6483453
55. Thurner L, Scheidler A, Schafer F et al (2018) Pandapower—an open-source python tool for convenient modeling, analysis, and optimization of electric power systems. IEEE Transactions on Power Systems 33(6):6510–6521. https://doi.org/10.1109/TPWRS.2018.2829021
56. Tomik S (2023) Balkonkraftwerk: Strom selbst erzeugen mit Steckersolargeräten und Photovoltaik auf Balkon, Terrasse und im Garten [Balcony Power Plant: Generate Your Own Electricity with Plug-in Solar Devices and Photovoltaics on Balcony, Terrace, and in the Garden]. Ulmer Eugen Verlag, Stuttgart, Germany
57. Tonkoski R, Turcotte D, El-Fouly THM (2012) Impact of high PV penetration on voltage profiles in residential neighborhoods. IEEE Transactions on Sustainable Energy 3:518–527. https://doi.org/10.1109/tste.2012.2191425
58. Turitsyn K, Sulc P, Backhaus S et al (2011) Options for control of reactive power by distributed photovoltaic generators. Proceedings of the IEEE 99(6):1063–1073. https://doi.org/10.1109/JPROC.2011.2116750
59. Vargas MC, Mendes MA, Batista OE (2018) Impacts of high PV penetration on voltage profile of distribution feeders under brazilian electricity regulation. In: 2018 13th IEEE International Conference on Industry Applications (INDUSCON). IEEE, Sao Paulo, pp 38–44, https://doi.org/10.1109/INDUSCON.2018.8627070
60. VDE (2018) Generators connected to the low-voltage distribution network - Technical requirements for the connection to and parallel operation with low-voltage distribution networks. VDE-AR-N 4105:2018-11 (Revision of VDE-AR-N 4105:2011-08) 2(1):1–96
61. Wang J, Luo F, Ji Z et al (2018) An Improved Hybrid Modulation Method for the Single-Phase H6 Inverter With Reactive Power Compensation. IEEE Transactions on Power Electronics 33(9):7674–7683. https://doi.org/10.1109/TPEL.2017.2768572
62. Wang L, Xie L, Yang Y et al (2023) Distributed online voltage control with fast pv power fluctuations and imperfect communication. IEEE Transactions on Smart Grid 14(5):3681–3695. https://doi.org/10.1109/tsg.2023.3236724

63. Zeraati M, Golshan MEH, Guerrero JM (2018) Distributed control of battery energy storage systems for voltage regulation in distribution networks with high PV penetration. IEEE Transactions on Smart Grid 9(4):3582–3593. https://doi.org/10.1109/TSG.2016.2636217

Publisher's Note